Monthly Notices
of the
ROYAL ASTRONOMICAL SOCIETY

Mon. Not. R. Astron. Soc. **404,** 433–441 (2010) doi:10.1111/j.1365-2966.2010.16286.x

A multifrequency study of the large radio galaxies 3C46 and 3C452

S. Nandi,[1⋆] A. Pirya,[1⋆] S. Pal,[2,3⋆] C. Konar,[4⋆] D. J. Saikia[2,3,5⋆] and M. Singh[1⋆]

[1]*Aryabhatta Research Institute of Observational Sciences (ARIES), Manora Peak, Nainital 263 129, India*
[2]*International Centre for Radio Astronomy Research, The University of Western Australia, Crawley WA 6009, Australia*
[3]*National Centre for Radio Astrophysics, TIFR, Pune University Campus, Post Bag 3, Pune 411 007, India*
[4]*Indian Institute of Astrophysics, Sarjapur Road, Koramangala, Bangalore 560 034, India*
[5]*Australia Telescope National Facility, CSIRO, PO Box 76, Epping NSW 1710, Australia*

Accepted 2010 January 5. Received 2009 December 21; in original form 2009 September 4

ABSTRACT

We present low-frequency observations starting from ∼150 MHz with the Giant Metrewave Radio Telescope, and high-frequency observations with the Very Large Array of two large radio galaxies 3C46 and 3C452. These observations were made with the objectives of estimating their spectral ages and examining any evidence of diffuse extended emission at low radio frequencies due to an earlier cycle of activity. While no evidence of extended emission due to an earlier cycle of activity has been found, the spectral ages have been estimated to be ∼15 and 27 Myr for the oldest relativistic plasma seen in the regions close to the cores for 3C46 and 3C452, respectively. The spectra in the vicinity of the hotspots are consistent with a straight spectrum with injection spectral indices of ∼1.0 and 0.78, respectively, somewhat steeper than theoretical expectations.

Key words: galaxies: active – galaxies: jets – galaxies: nuclei – quasars: general – radio continuum: galaxies.

1 INTRODUCTION

Large double-lobed radio galaxies, the largest of which are the giant radio sources (GRSs), defined to be those which have a projected linear size $\gtrsim$1 Mpc ($H_0 = 71\,\mathrm{km\,s^{-1}\,Mpc^{-1}}$, $\Omega_\mathrm{m} = 0.27$, $\Omega_\mathrm{vac} = 0.73$; Spergel et al. 2003), are useful for studying the late stages of evolution of radio sources and possible episodic activity in these objects, constraining orientation-dependent unified schemes and probing the intergalactic medium at different redshifts (e.g. Subrahmanyan & Saripalli 1993; Subrahmanyan, Saripalli & Hunstead 1996; Mack et al. 1998; Blundell, Rawlings & Willott 1999 and references therein; Ishwara-Chandra & Saikia 1999; Kaiser & Alexander 1999; Schoenmakers et al. 2000, 2001; Singal, Konar & Saikia 2004). In addition, large radio sources are useful for studying the effects of electron energy loss in the lobe plasma due to inverse-Compton scattering with the cosmic microwave background radiation (CMBR) photons at different redshifts (e.g. Konar et al. 2004), making independent estimates of the magnetic field from the inverse-Compton scattered X-ray flux density from the lobes (e.g. Croston et al. 2005; Konar et al. 2009) and spectral as well as dynamical ageing analyses to understand the evolution of the sources (e.g. Konar et al. 2006, 2008; Jamrozy et al. 2008; Machalski, Jamrozy & Saikia 2009).

We have selected two large radio galaxies with prominent bridges, 3C46 and 3C452, for making detailed radio images with the Giant Metrewave Radio Telescope (GMRT) at low frequencies going down to ∼150 MHz. We have also used archival Very Large Array (VLA) data to make higher frequency images of these two sources. The twin objectives of this study were to look for diffuse emission at low frequencies from an earlier cycle of activity and estimate the spectral ages of the lobes from data over a large frequency range. Combining the lowest frequency available data with high-frequency data gives the most reliable estimates of the injection spectral indices (α_inj), and also spectral ages from the break frequency. For examining emission from an earlier cycle of activity, it is relevant to note that evidence of episodic activity is seen usually in large radio sources (e.g. Schoenmakers et al. 2000; Saikia, Konar & Kulkarni 2006, and references therein) but not in the small sources even at low radio frequencies (Sirothia et al. 2009).

The radio galaxy 3C46 (J0135+3754), which has a very close companion galaxy (de Vries et al. 1998), is at a redshift of 0.4373 (Smith & Spinrad 1980) and has a largest angular size of ∼150 arcsec which corresponds to 846 kpc, and a total radio luminosity of $\log P_{1.4\,\mathrm{GHz}}\,(\mathrm{W\,Hz^{-1}}) = 27.01$ (Konar et al. 2004). VLA B- and C-array images at *L* band (Gregorini et al. 1988; Vigotti et al. 1989) and the D-array image at *C* band (Konar et al. 2004) show the extended lobes of emission with an edge-brightened structure. de Koff et al. (2000) report evidence of a dust lane lying across the nucleus with the radio axis being nearly perpendicular to it.

⋆E-mail: sumana@aries.res.in (SN); akash@aries.res.in (AP); spal@cyllene.uwa.edu.au (SP); chiranjib.konar@gmail.com (CK); djs@ncra.tifr.res.in, Dhruba.Saikia@csiro.au (DJS); msingh@aries.res.in (MS)

3C452 (J2245+3941) is at a redshift of 0.0811 (Schmidt 1965), and has a moderately strong core with a flux density of 130 mJy at 5 GHz (Riley & Pooley 1975), and two edge-brightened lobes separated by 252 arcsec which corresponds to 381 kpc. The total radio luminosity at 1.4 GHz is log $P_{1.4\,\mathrm{GHz}}$ (W Hz^{-1}) = 26.53. There is a suggestion of a faint dust lane near the nucleus leading to the dumbbell shape (de Koff et al. 2000). The axis defined by the radio lobes and the core is perpendicular to the proposed dust lane. Very long baseline interferometric observations of the nuclear source show a reasonably symmetric structure with the central peak being identified with the core. The jet symmetry and the prominence of the possible core suggest that the source is oriented at an angle larger than $\sim 60^\circ$ to the line of sight (Giovannini et al. 2001). Gupta & Saikia (2006) have reported the discovery of H I absorption towards the radio core of 3C452 from GMRT observations of the source.

Table 1. Observing log.

Source	Telescope	Array Conf.	Obs. Freq. (MHz)	Phase Calib.	Obs. Date
(1)	(2)	(3)	(4)	(5)	(6)
3C46	GMRT		153	3C48	2007 Dec 07
3C46	GMRT		240	3C48	2007 Jun 09
3C46	GMRT		332	3C48	2008 Feb 23
3C46	GMRT		606	3C48	2007 Jun 09
3C46	VLA[a]	B and C	1465	2254+247	2000 Mar 13
3C46	VLA[a]	D	4841	2250+143	2000 Jul 24
3C46	VLA[a]	D	8460	2251+158	1998 Jan 24
3C452	GMRT		153	2350+646	2007 Dec 08
3C452	GMRT		240	2350+646	2005 May 30
3C452	GMRT		332	2350+646	2008 Jan 02
3C452	GMRT		606	2350+646	2005 May 30
3C452	GMRT		1314	2202+422	2005 Dec 10
3C452	VLA[a]	D	4910	2253+417	1995 Apr 11
3C452	VLA[a]	D	8350	2255+420	1995 Apr 11

[a]Archival data from the VLA.

2 OBSERVATIONS AND ANALYSES

Both the GMRT and the VLA observations were made in the standard fashion, with each target source observations interspersed with observations of the phase calibrator. The primary flux density and bandpass calibrator was 3C48 and/or 3C286 at the different frequencies, with all flux densities being on the scale of Baars et al. (1977). The total observing time on the source is about a few hours for the GMRT observations while for the VLA observations the time on source ranges from a few minutes to $\sim$10 min. The low-frequency GMRT data were sometimes significantly affected by radio frequency interference, and these data were flagged. All the data were analysed in the standard fashion using the National Radio Astronomy Observatory (NRAO) AIPS package. For the GMRT observations, besides flagging bad data, the steps followed include gain calibration of one spectral channel data, bandpass calibration and

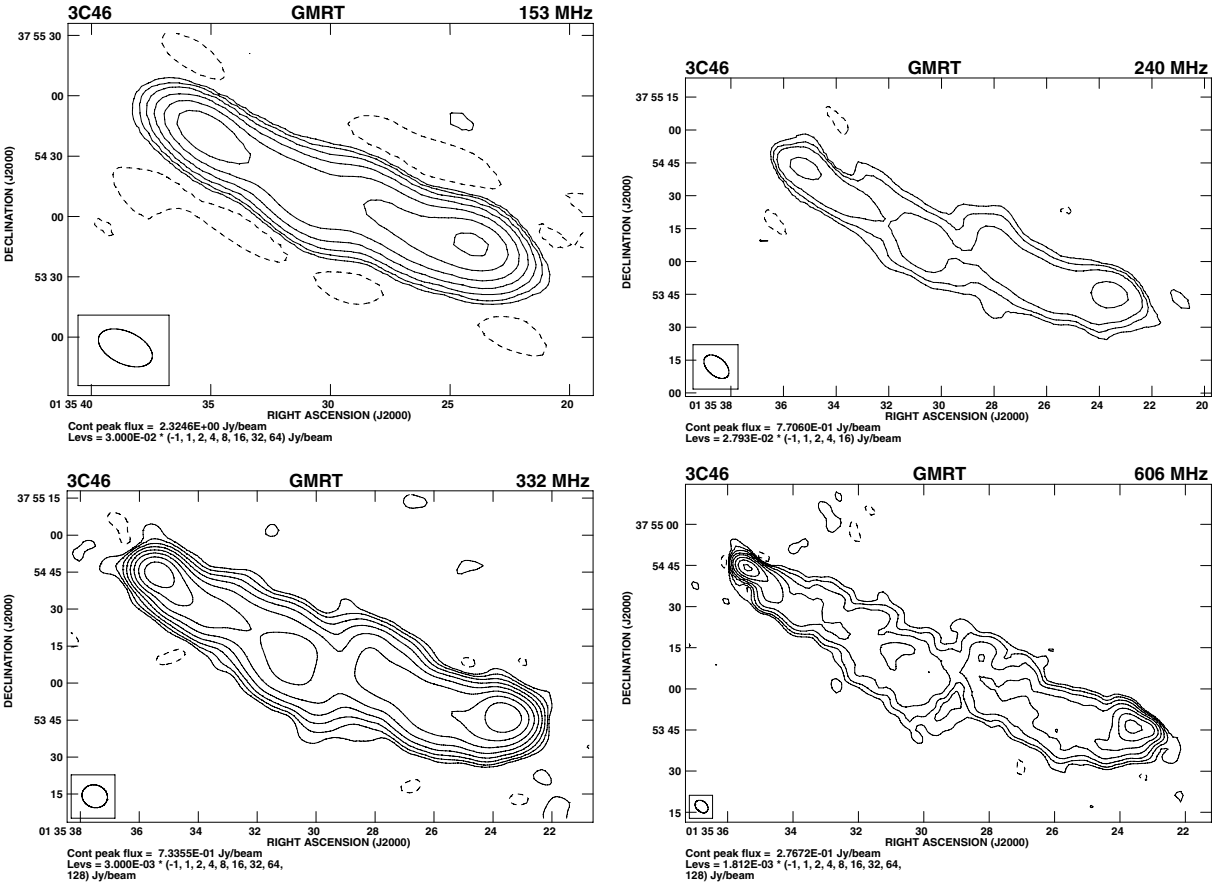

Figure 1. GMRT low-frequency images of 3C46 at 153, 240, 332 and 606 MHz, and VLA higher frequency images at 1465, 4841 and 8460 MHz. In this figure as well as in all the other images of the sources, the peak brightness and the contour levels are given below each image. In all the images, the restoring beam is indicated by an ellipse.

channel averaging to obtain the continuum data base. These were then imaged and cleaned using multiple facets for the different low-frequency GMRT observations. All the data were self-calibrated to produce the final images, which were then corrected for the gain of the primary beam.

The observing log for both the GMRT and the VLA observations is given in Table 1 which is arranged as follows. Columns 1 and 2 show the name of the source and the telescope; Column 3 gives the array configuration for the VLA observations; Column 4 shows the frequency of the observations in MHz; Column 5 lists the phase calibrators used for the different observations, while Column 6 lists the dates of the observations. For the VLA observations of 3C452 at 8350 MHz, there were two sets of observations, one pointed towards each lobe.

3 OBSERVATIONAL RESULTS

The GMRT and VLA images of 3C46 are presented in Fig. 1 while those of 3C452 are presented in Fig. 2. The observational parameters

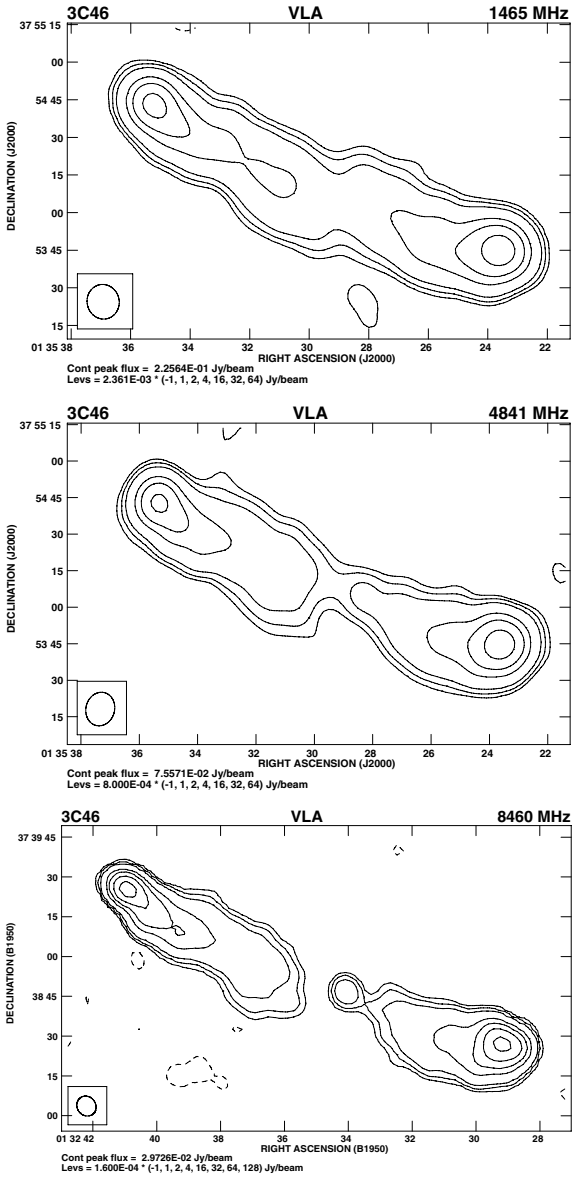

Figure 1 – *continued*

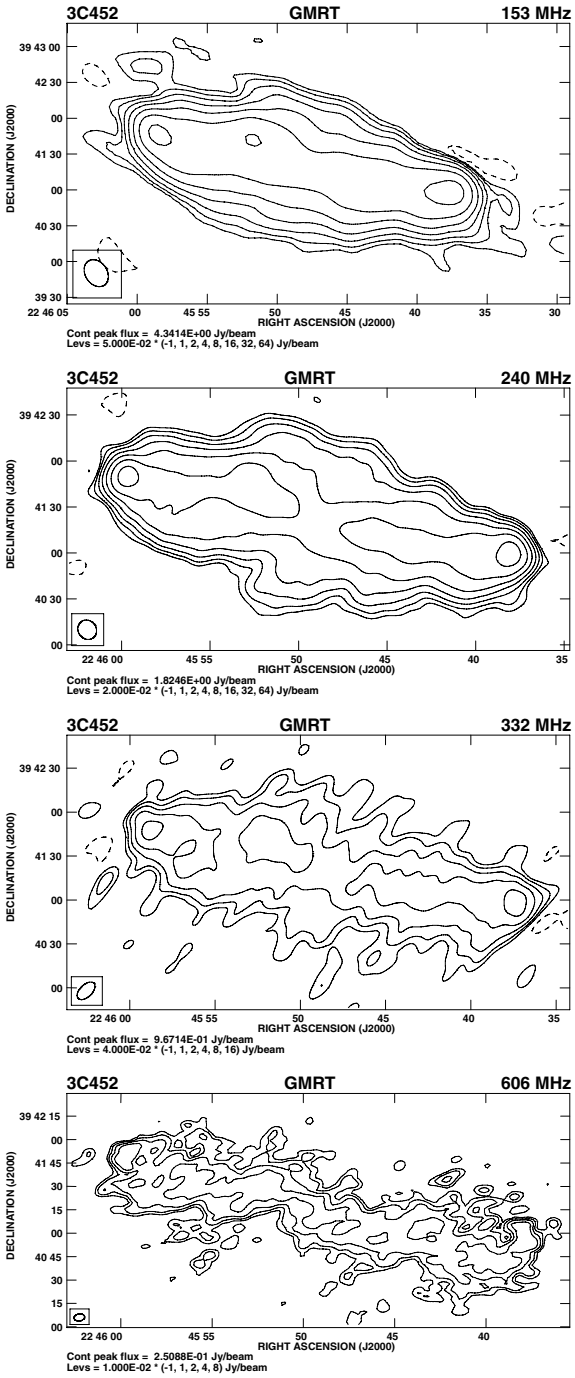

Figure 2. GMRT low-frequency images of 3C452 at 153, 240, 332, 606 and 1314 MHz, and VLA higher frequency images at 4910 and 8350 MHz. For the images at 8350 MHz, in the case of 3C452W the pointing centre was towards the western hotspot, while in the case of 3C452E the pointing centre was towards the eastern hotspot.

and some of the observed properties are presented in Table 2, which is arranged as follows. Column 1: name of the source; Column 2: frequency of observations in units of MHz, with the letter G or V representing either GMRT or VLA observations; Columns 3–5: the major and minor axes of the restoring beam in arcsec and its position angle in degrees; Column 6: the rms noise in units of mJy beam^{-1}; Column 7: the integrated flux density of the source in mJy. We examined the change in flux density by specifying different areas

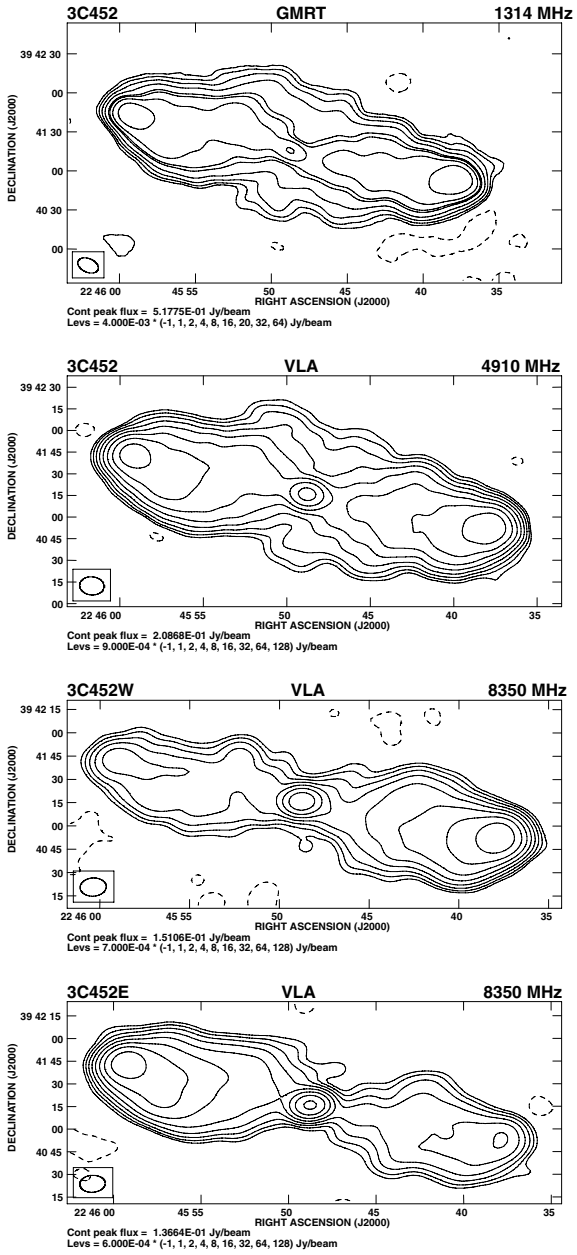

Figure 2 – *continued*

around the source and found the difference to be within a few per cent. The flux densities at different frequencies have been estimated over similar areas. Columns 8, 11 and 14: component designation, where W, E and C denote the western, eastern and core components, respectively; Columns 9 and 10, 12 and 13, and 15 and 16: the peak and total flux densities of each of the components in units of mJy beam^{-1} and mJy, respectively. For the 8350-MHz observations of 3C452, the flux density of the lobe which was at the pointing centre is reliable and has been listed. The superscript *g* indicates that the flux densities have been estimated from a two-dimensional Gaussian fit to the core component. The spectra of the extended emission after subtracting the core flux density at frequencies larger than ∼1400 MHz are shown in Fig. 3 along with the fits to the data using the SYNAGE package (Murgia et al. 1999). The total flux densities are from Laing & Peacock (1980) and our measurements.

4 DISCUSSION AND RESULTS

4.1 Radiative losses

In the high-luminosity Fanaroff–Riley type II (FR II) radio sources, as the jets of relativistic plasma traverse outwards initially through the interstellar medium of the host galaxy and later through the intracluster and intergalactic medium, they dissipate their energy at their leading edges. This gives rise to the intense regions of emission called 'hotspots'. The relativistic particles flow out from the hotspots to form the extended lobes of radio emission, so that the radiating particles closest to the hotspot are the youngest while those farthest from it are the oldest. The radio continuum spectra in different parts of an extended radio source contain information about the various energy losses and gains of the radiating particles during the lifetime of the source. If there is no significant reacceleration within these lobes and no significant mixing of particles, there should be a spectral gradient across the radio source. The hotspots where the particles are being accelerated should have the flattest spectral index, reflecting the injection spectral index $\alpha_{\rm inj}$, while the spectrum should steepen with increasing distance from the hotspot. Since the high-energy particles lose energy more rapidly, the steepening in the spectrum would be seen more clearly at high frequencies. This trend has been reported in several studies and used to estimate the radiative ages and expansion velocities in the powerful 3CR sources (e.g. Myers & Spangler 1985; Alexander & Leahy 1987; Leahy, Muxlow & Stephens 1989; Carilli et al. 1991; Liu, Pooley & Riley 1992), in the low-luminosity and medium-luminosity radio galaxies (e.g. Klein et al. 1995; Parma et al. 1999), GRSs (Jamrozy et al. 2008, and references therein; Konar et al. 2008) and compact steep-spectrum sources (Murgia et al. 1999). However, there are several caveats in the interpretation which one needs to bear in mind. These include details of the backflow of the lobe material, difficulties in disentangling the different energy losses of the radiating particles and variations of the local magnetic field (e.g. Wiita & Gopal-Krishna 1990; Rudnick, Katz-Stone & Anderson 1994; Eilek & Arendt 1996; Jones, Ryu & Engel 1999; Blundell & Rawlings 2000).

Nevertheless, these provide useful inputs towards understanding the different physical processes which play a role in the evolution of these radio sources. The large radio sources are particularly suitable for the classical spectral ageing analysis due to their large angular extent which can be covered by a significant number of resolution elements. Combining low-frequency information from the GMRT along with high-frequency ones from the VLA is likely to yield the most reliable estimates of the spectral break frequency, as has been demonstrated in a number of recent studies (Jamrozy et al. 2008 and references therein; Konar et al. 2008).

4.2 Spectral ageing analysis

The observed spectra have been fitted using the Jaffe & Perola (1973, JP) and the Kardashev–Pacholczyk (Kardashev 1962; Pacholczyk 1970; KP) models using the SYNAGE package (Murgia et al. 1999). As reported by Jamrozy et al. (2008), there is no significant difference between these two models over the frequency range of our observations, and the JP model tends to give a better fit to the different strips in the lobes than with the continuous injection (Kardashev 1962; CI) model. The CI model sometimes gives a somewhat better fit in the area of a prominent hotspot, but since with the resolution of our observations the flux density of the hotspots are contaminated by lobe emission it does not make a significant difference.

Table 2. The observational parameters and observed properties of the sources.

Source	Freq.	Beam size			rms	S_I	Cp	S_p	S_t	Cp	S_p	S_t	Cp	S_p	S_t
	(MHz)	(arcsec)	(arcsec)	(°)	(mJy beam^{-1})	(mJy)		(mJy beam^{-1})	(mJy)		(mJy beam^{-1})	(mJy)		(mJy beam^{-1})	(mJy)
(1)	(2)	(3)	(4)	(5)	(6)	(7)	(8)	(9)	(10)	(11)	(12)	(13)	(14)	(15)	(16)
3C46	G153	28.5	16.0	65	6.9	10880	W	2325	6029	C			E	1852	4899
	G240	13.2	8.1	48	4.3	6806	W	771	3821	C			E	721	3099
	G332	10.3	9.1	69	0.54	5957	W	725	3172	C			E	734	2689
	G606	5.2	3.8	48	0.23	2051	W	157	1537	C			E	277	1402
	V1465	13.8	12.7	12	0.61	1202	W	253	640	C			E	197	590
	V4841	13.9	11.6	166	0.15	355	W	76	185	C[g]	1.2	1.1	E	60	172
	V8460	7.7	6.9	32	0.04	183	W	25	88	C[g]	1.6	1.8	E	30	94
3C452	G153	24.1	18.1	32	8.7	81142	W	4341	38725	C			E	3909	42366
	G240	13.1	11.8	34	4.5	55706	W	1810	27589	C			E	1825	28422
	G332	14.9	8.3	134	2.6	37703	W	967	18191	C			E	862	18724
	G606	6.7	4.4	98	0.68	24369	W	207	11246	C			E	251	11893
	G1313	16.4	10.5	65	0.92	11565	W	518	5110	C[g]	213	203	E	503	5677
	V4910	17.0	12.6	85	0.44	3318	W	209	1435	C[g]	153	213	E	188	1399
	V8350W	16.8	11.7	94	0.06	1860	W	151	860	C[g]	121	145	E		
	V8350E	16.8	11.2	93	0.07	1865	W			C[g]	134	151	E	137	816

Assuming that (i) the magnetic field strength in a given strip is constant throughout the energy-loss process, (ii) the particles injected into the lobe have a constant power-law energy spectrum with an index γ and (iii) the time-scale of isotropization of the pitch angles of the particles is short compared with their radiative lifetime, the spectral age, $\tau_{\rm spec}$, is given by

$$\tau_{\rm spec} = 50.3 \frac{B^{1/2}}{B^2 + B_{\rm iC}^2} [\nu_{\rm br}(1+z)]^{-1/2} \,({\rm Myr}), \quad (1)$$

where $B_{\rm iC} = 0.318(1+z)^2$ is the magnetic field strength equivalent to the CMBR. Here B, the magnetic field strength of the lobes, and $B_{\rm iC}$ are expressed in units of nT, $\nu_{\rm br}$ is the spectral break frequency in GHz above which the radio spectrum steepens from the initial power-law spectrum given by $\alpha_{\rm inj} = (\gamma - 1)/2$. Alexander & Leahy (1987) and Alexander (1987) have suggested that the effects of expansion losses may be neglected.

To estimate the values of $\alpha_{\rm inj}$ for the two sources, we fit the JP model to the flux densities of the entire lobes, treating $\alpha_{\rm inj}$ as a free parameter, as well as the total flux density measurements of the source which go to lower frequencies (Laing & Peacock 1980) than our measurements. These yield injection spectral indices of 1.00 and 0.78 for 3C46 and 3C452, respectively (Fig. 3). Having estimated the $\alpha_{\rm inj}$ values, the total-intensity images of 3C46 and 3C452 have been convolved to a common resolution of 14 and 17 arcsec, respectively, to be consistent with the lowest resolution image for all images at ∼240 MHz and above. The 150-MHz images have not been used for this analysis since their resolution is coarser by another factor of 2, and we wish to have at least ∼10 resolution elements along the axis of the source. Each lobe is then split into a number of strips as shown in Fig. 4, separated approximately by the resolution element along the axis of the source, and also ensuring that the core component lies between two vertical lines and can be subtracted reliably. The extreme strips are centred at the peaks of brightness on the convolved maps. Both these sources have prominent bridges of emission, and we have also fitted the spectrum to the central region of the source after subtracting the flux density of the radio core. Using the SYNAGE software, we determine the best fit to the spectrum in each strip from ∼240 to 8000 MHz using the JP model, and derive the relevant value of $\nu_{\rm br}$. A few examples of the fits to the different strips of both the lobes in 3C46 and 3C452 are presented in Figs 5 and 6, respectively, while the fits to the central regions of the source, which as expected show the lowest values of $\nu_{\rm br}$, are presented in Fig. 7.

In order to estimate the spectral ages, we have to estimate the magnetic field strength. We have estimated the magnetic field strength by integrating the spectrum from a frequency corresponding to a minimum Lorentz factor, $\gamma_{\rm min} \sim 10$, for the relativistic electrons to an upper limit of 100 GHz, which corresponds to a Lorentz factor ranging from a few times 10^4 to 10^5 depending on the estimated magnetic field strength (see Hardcastle et al. 2004; Croston et al. 2005; Konar et al. 2008; Konar et al. 2009). It has also been assumed that the filling factors of the lobes are unity, and the energetically dominant particles are the radiating particles only, neglecting the contribution of the protons. We have assumed a cylindrical geometry for the entire lobe, and have estimated the magnetic field for the entire lobe as well as for individual strips of emission each separated by approximately a beamwidth along the long axis of each source. The magnetic field strengths for each strip are listed in Tables 3 and 4 for 3C46 and 3C452, respectively. The magnetic field strengths for the western and eastern lobes of 3C46 are 1.66 and 1.53 nT while the corresponding values for 3C452 are 0.86 and 0.88 nT, respectively. The equipartition magnetic fields are usually within a factor of 2 of those estimated from inverse-Compton scattering of the radiating electrons by the microwave background radiation (e.g. Croston et al. 2005; Konar et al. 2009). For the GRS 3C457, the spectral ages estimated from the equipartition magnetic field and the field estimated from the inverse-Compton scattered X-ray emission are similar (Konar et al. 2009).

The results of our spectral ageing analysis for 3C46 and 3C452 are tabulated in Tables 3 and 4, respectively, which are arranged as follows. Column 1: identification of the strip, Column 2: projected distance of the centre of the strip from the radio core in units of kpc, Column 3: break frequency of the spectrum of the strip according to the JP model in units of GHz, Column 4: reduced χ^2 value of the fit, Column 5: magnetic field strength in units of nT and Column 6: spectral age of particles in the strip. The strips close to the hotspots are consistent with having straight spectra and the SYNAGE fits yield spectral breaks at frequencies larger than several hundred GHz. Our observations show no spectral break till ∼10 GHz. In Tables 3 and 4, we have listed the values corresponding to a break

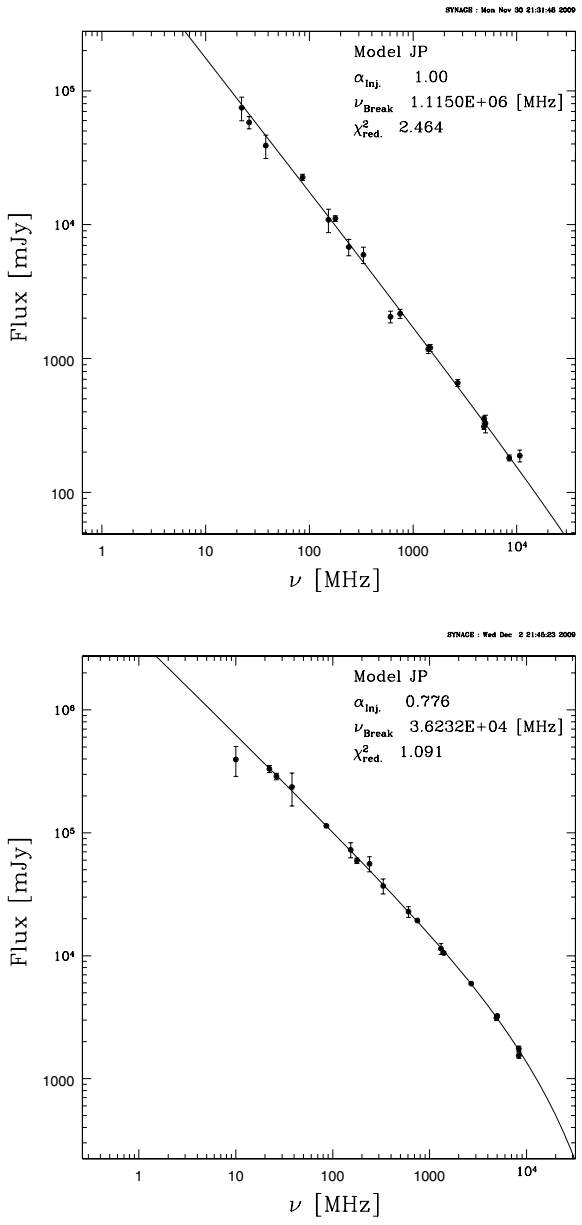

Figure 3. The spectra of the extended emission of 3C46 (upper panel) and 3C452 (lower panel) obtained after subtracting the core flux density at frequencies greater than ∼1400 MHz from the total flux density. Any contributions of the core flux density at lower frequencies are less than ∼1 per cent and have been neglected. The total flux densities are from Laing & Peacock (1980) and the measurements presented in this paper. The fits to the spectra obtained using the SYNAGE package (Murgia et al. 1999) are also shown.

frequency of 100 GHz for these strips. Observations at millimetre wavelengths are required to determine reliably the spectral breaks in these regions. The spectral age increases with distance from the hotspot for both sources, with the maximum spectral ages estimated for 3C46 and 3C452 being ∼15 and 27 Myr in the regions closest to the core (Fig. 8).

4.3 Search for episodic activity

The outer diffuse lobes from an earlier cycle of activity in sources with episodic activity are expected to have a steep spectra due to

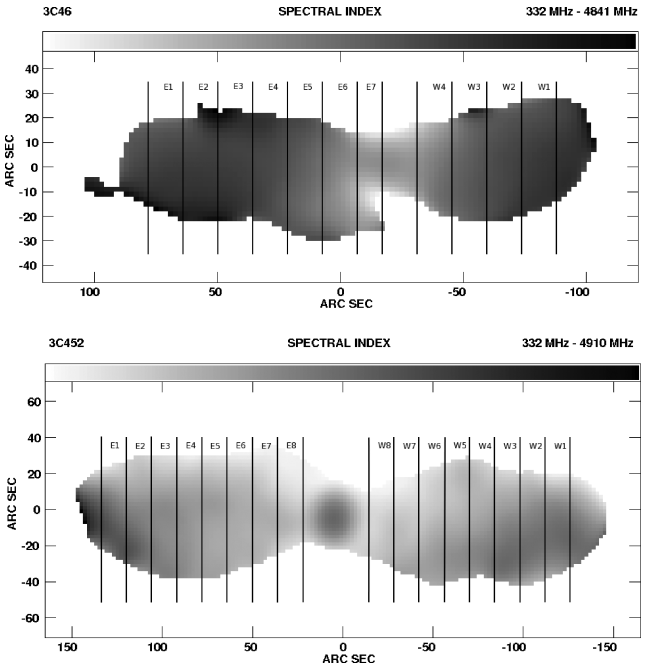

Figure 4. The spectral-index images of 3C46 and 3C452 with the strips used for estimating the spectral ages along the lobes being marked by vertical lines and labelled. The central region corresponds to the 'central core' region in Tables 3 and 4 and Fig. 8. The images have been rotated so that they lie in the east-west direction. The spectral indices have been estimated between 332 and ∼5000 MHz. The grey-scale bar indicates variations in spectral index from 0.4 to 2.0 for 3C46 and −0.4 to 1.4 for 3C452. Some of the values at the edges are spurious.

radiative and adiabatic losses. This has been observationally demonstrated in some cases such as J1453+3308 (Konar et al. 2006) and 4C29.30 (Jamrozy et al. 2008). Therefore, ideally one should be able to detect these features more easily at low frequencies. Our low-frequency images show the prominent bridges of emission but no diffuse features that could be attributed to an earlier cycle of activity. In the case of 3C46, a diffuse component of say ∼20 mJy at 153 MHz and a spectral index of 1 would have a surface brightness similar to the rms noise in the 8460-MHz image. The corresponding value for 3C452 is ∼8 mJy at 153 MHz. These values would increase by a factor of ∼2 and 7 for spectral indices of 1.2 and 1.5, respectively. With the rms noise values of 6.9 and 8.7 mJy beam^{-1} at 153 MHz for 3C46 and 3C452, respectively, diffuse emission not seen at the highest frequency could have been just about detected in 3C46. However, for 3C452 only steeper spectrum emission with a spectral index of ∼1.4 could have been detected. While it is important to make more sensitive images at the lowest frequencies, the non-detection of extended emission due to an earlier cycle of activity in these two sources is consistent with the trend that such objects are rare even amongst large radio sources (cf. Schoenmakers et al. 2000; Saikia et al. 2006).

5 CONCLUDING REMARKS

The maximum spectral ages determined for 3C46 and 3C452 are ∼15 and 27 Myr, respectively, which is similar to the values of Jamrozy et al. (2008) obtained for a sample of 10 large radio galaxies by combining GMRT and VLA data. Their values range from ∼6 to 36 Myr with a median value of ∼20 Myr using the classic equipartition magnetic fields. These estimates are significantly

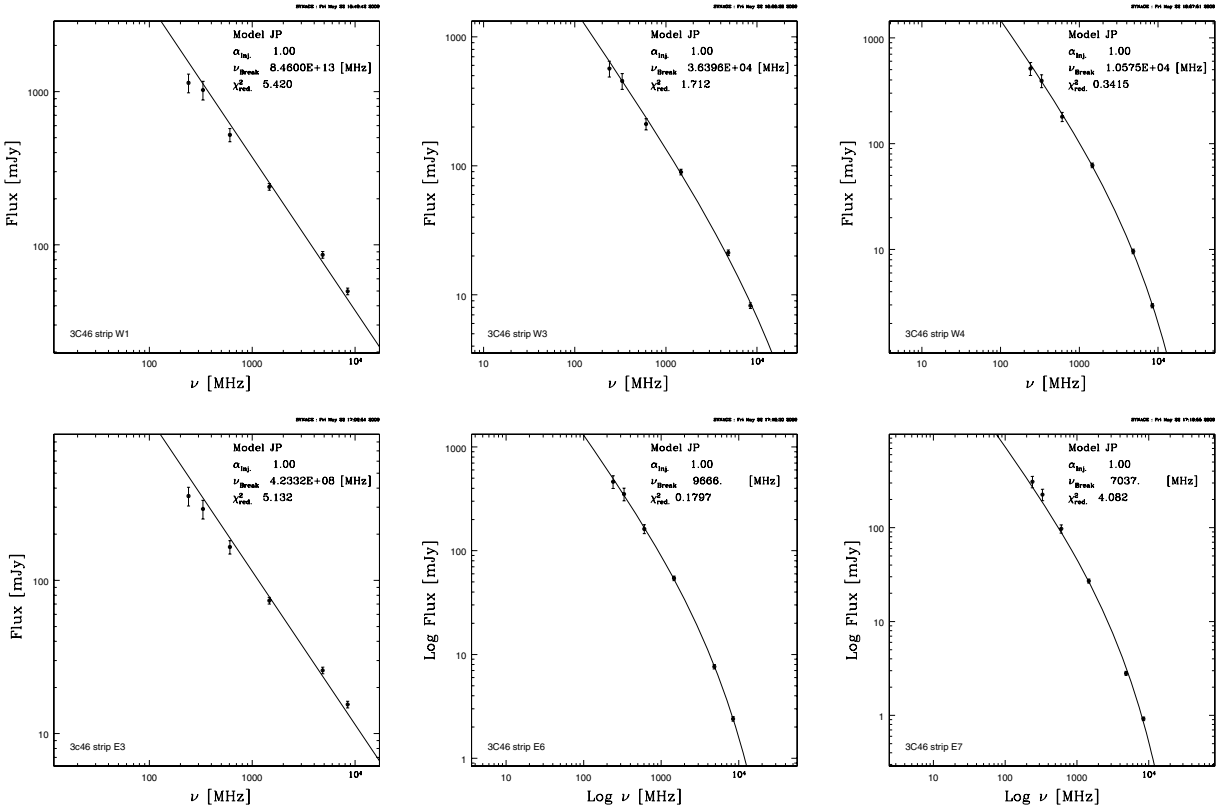

Figure 5. Typical spectra of the strips for the western (upper panel) and eastern (lower panel) lobes of 3C46, with the fits from the JP model as described in the text.

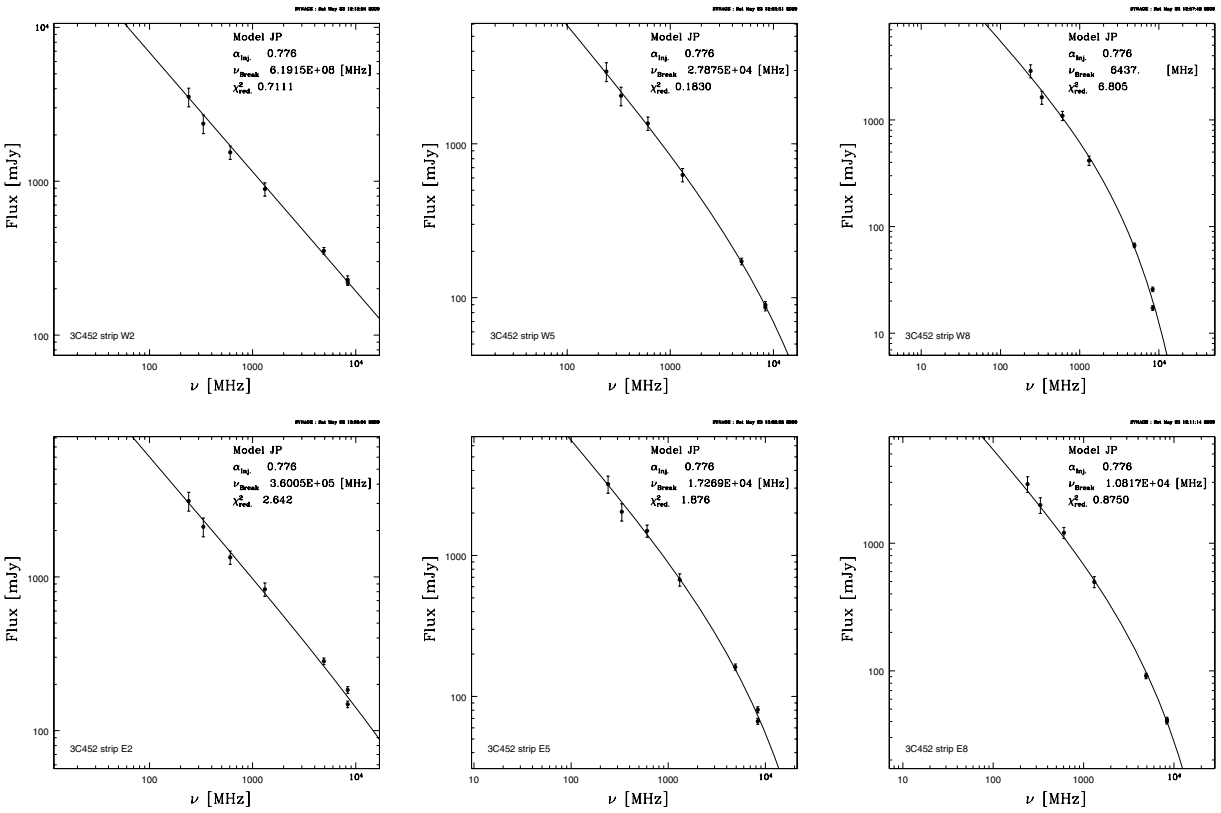

Figure 6. Typical spectra of the strips for the western (upper panel) and eastern (lower panel) lobes of 3C452, with the fits from the JP model as described in the text.

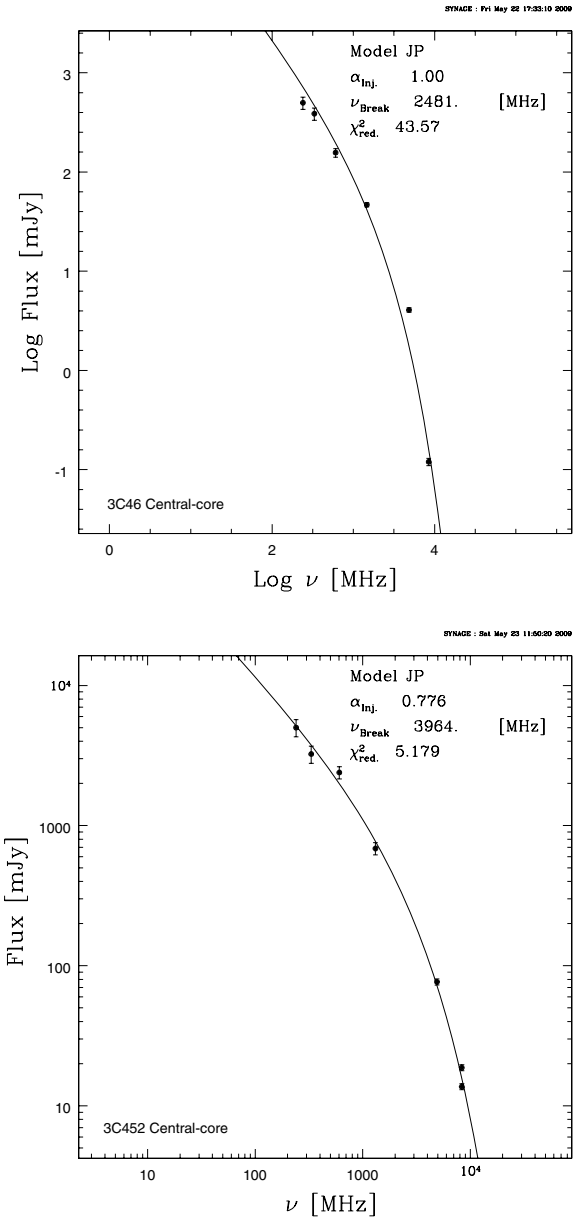

Figure 7. Spectra of the central regions of 3C46 (upper panel) and 3C452 (lower panel) after subtraction of the core flux density, with the fits from the JP model as described in the text.

Table 3. Estimates of break frequency and spectral age for 3C46.

Strip	Dist. (kpc)	ν_{br} (GHz)	χ^2_{red}	B (nT)	τ_{spec} (Myr)
		Western lobe		$\alpha_{inj} = 1.0$	
W1	316	>100	5.42	1.64	<1.7
W2	237	>100	1.78	1.35	<2.2
W3	158	$36.4^{+6.5}_{-28.3}$	1.71	1.35	$3.6^{+4.1}_{-0.4}$
W4	79	$10.6^{+0.7}_{-3.9}$	0.34	1.34	$6.7^{+1.7}_{-0.2}$
		Eastern lobe		$\alpha_{inj} = 1.0$	
E1	519	>100	10.2	1.50	<1.9
E2	440	>100	11.4	1.36	<2.2
E3	361	>100	5.1	1.20	<2.4
E4	282	>100	1.0	1.12	<2.6
E5	203	$36.3^{>+6.6}_{-25.8}$	0.9	1.26	$3.9^{+3.3}_{-0.3}$
E6	124	$9.7^{>+0.6}_{-2.2}$	0.2	1.30	$7.3^{+1.0}_{-0.2}$
E7	56	$7.0^{>+0.4}_{-0.3}$	4.1	1.22	$9.1^{+0.2}_{-0.3}$
		Central core		$\alpha_{inj} = 1.0$	
		$2.5^{+0.05}_{-0.7}$	44	1.28	$14.5^{+2.6}_{-0.1}$

Table 4. Estimates of break frequency and spectral age for 3C452.

Strip	Dist. (kpc)	ν_{br} (GHz)	χ^2_{red}	B (nT)	τ_{spec} (Myr)
		Western lobe		$\alpha_{inj} = 0.776$	
W1	197	>100	9.87	0.76	<5.9
W2	173	>100	0.71	0.83	<5.4
W3	150	>100	0.71	0.79	<5.6
W4	126	$68.8^{+24.7}_{-36.1}$	0.49	0.77	$7.0^{+3.2}_{-1.0}$
W5	103	$27.9^{+28.3}_{-11.7}$	0.18	0.80	$10.6^{+3.3}_{-3.1}$
W6	79	$13.6^{+3.4}_{-5.3}$	1.12	0.81	$14.9^{+4.2}_{-1.6}$
W7	56	$7.7^{+0.5}_{-3.8}$	3.71	0.82	$19.6^{+7.9}_{-0.6}$
W8	32	$6.4^{+0.8}_{-1.4}$	8.81	0.80	$22.1^{+2.9}_{-1.3}$
		Eastern lobe		$\alpha_{inj} = 0.776$	
E1	194	>100	8.30	0.76	<5.9
E2	171	>100	2.64	0.80	<5.6
E3	147	$60.2^{+34.2}_{-48.8}$	3.13	0.82	$6.9^{+9.0}_{-1.4}$
E4	123	$25.6^{+4.8}_{-18.9}$	5.47	0.83	$10.5^{+10.0}_{-0.9}$
E5	100	$17.3^{+4.0}_{-8.6}$	1.88	0.83	$12.9^{+5.3}_{-1.3}$
E6	76	$13.1^{+5.2}_{-3.6}$	0.22	0.84	$14.5^{+2.5}_{-2.3}$
E7	53	$9.8^{+2.3}_{-2.07}$	0.53	0.83	$17.1^{+2.2}_{-1.7}$
E8	29	$10.8^{+35.0}_{-0.9}$	0.88	0.79	$17.3^{+0.7}_{-8.9}$
		Central core		$\alpha_{inj} = 0.776$	
		$3.96^{+0.2}_{-0.8}$	5.18	0.83	$26.8^{+3.2}_{-0.6}$

older than those of smaller sources (e.g. Leahy et al. 1989; Liu et al. 1992), and broadly consistent with the tendency for spectral age to increase with the projected linear size (Jamrozy et al. 2008 and references therein).

The injection spectral indices are ∼1.0 and 0.78, compared with the values ranging from 0.55 to 0.88 with a median value of ∼0.6 for the sample of Jamrozy et al. (2008). Our estimates for 3C46 and 3C452, which have prominent hotspots, are consistent with the higher values in the sample of Jamrozy et al. (2008) and studies of smaller FR II sources studied by Leahy et al. (1989) and Liu et al. (1992). Our estimates of the injection spectral indices appear steeper than theoretically expected values for a strong, non-relativistic shock in a Newtonian fluid where $\alpha_{inj} = 0.5$ (Bell 1978a,b; Blandford & Ostriker 1978), or for different scenarios involving relativistic shocks where α_{inj} vary in the range of 0.35–0.65 (Drury & Völk 1981; Axford, Leer & McKenzie 1982; Kirk & Schneider 1987; Heavens 1989). High-resolution observations of these sources at even lower frequencies with future instruments should help in determining injection spectra more reliably.

ACKNOWLEDGMENTS

We thank an anonymous reviewer for a very detailed report which has improved the paper significantly. SN and AP thank NCRA, TIFR for hospitality during the course of this work and DST, Government

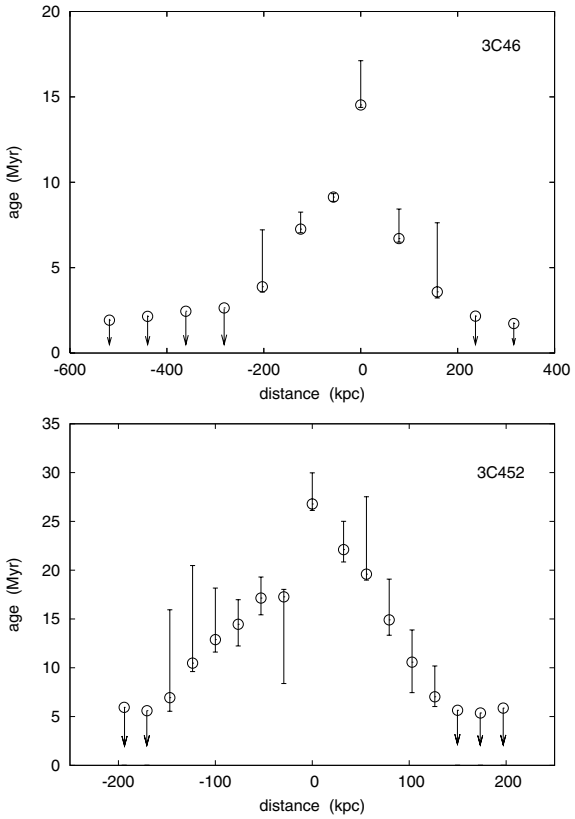

Figure 8. The spectral age is plotted against the distance from the core for 3C46 (upper panel) and 3C452 (lower panel) using the magnetic field estimated for each strip.

of India for financial support via Grant No. SR/S2/HEP-17/2005. We thank Neeraj Gupta for providing the calibrated *L*-band GMRT data on 3C452. The GMRT is a national facility operated by the National Centre for Radio Astrophysics of the Tata Institute of Fundamental Research. We thank the staff for help with the observations. The NRAO is a facility of the National Science Foundation operated under co-operative agreement by Associated Universities Inc. We thank the VLA staff for easy access to the archival data base. This research has made use of the NASA/IPAC extragalactic data base (NED) which is operated by the Jet Propulsion Laboratory, Caltech, under contract with the National Aeronautics and Space Administration. We thank numerous contributors to the GNU/Linux group.

REFERENCES

Alexander P., 1987, MNRAS, 225, 27
Alexander P., Leahy J. P., 1987, MNRAS, 225, 1
Axford W. I., Leer E., McKenzie J. F., 1982, A&A, 111, 317
Baars J. W. M., Genzel R., Pauliny-Toth I. I. K., Witzel A., 1977, A&A, 61, 99
Bell A. R., 1978a, MNRAS, 182, 147
Bell A. R., 1978b, MNRAS, 182, 443
Blandford R. D., Ostriker J. P., 1978, ApJ, 221, L29
Blundell K. M., Rawlings S., 2000, AJ, 119, 1111
Blundell K. M., Rawlings S., Willott C. J., 1999, AJ, 117, 677
Carilli C. L., Perley R. A., Dreher J. W., Leahy J. P., 1991, ApJ, 383, 554
Croston J. H., Hardcastle M. J., Harris D. E., Belsole E., Birkinshaw M., Worrall D. M., 2005, ApJ, 626, 733
de Koff S. et al., 2000, ApJS, 129, 33
de Vries W. H., O'Dea C. P., Perlman E., Baum S. A., Lehnert M. D., Stocke J., Rector T., Elston R., 1998, ApJ, 503, 138
Drury L. O'C., Völk J. H., 1981, ApJ, 248, 344
Eilek J. A., Arendt P. N., 1996, ApJ, 457, 150
Giovannini G., Cotton W. D., Feretti L., Lara L., Venturi T., 2001, ApJ, 552, 508
Gregorini L., Padrielli L., Parma P., Gilmore G., 1988, A&AS, 74, 107
Gupta N., Saikia D. J., 2006, MNRAS, 370, L80
Hardcastle M. J., Harris D. E., Worrall D. M., Birkinshaw M., 2004, ApJ, 612, 729
Heavens A., 1989, in Meisenheimer K., Röser H.-J., eds, Radio Hotspots in Extragalactic Radio Sources. Springer-Verlag, Heidelberg, p. 247
Ishwara-Chandra C. H., Saikia D. J., 1999, MNRAS, 309, 100
Jaffe W. J., Perola G. C., 1973, A&A, 26, 423
Jamrozy M., Konar C., Machalski J., Saikia D. J., 2008, MNRAS, 385, 1286
Jones T. W., Ryu D., Engel A., 1999, ApJ, 512, 105
Kaiser C. R., Alexander P., 1999, MNRAS, 302, 515
Kardashev N. S., 1962, SvA, 6, 317
Kirk J. G., Schneider P., 1987, ApJ, 315, 425
Klein U., Mack K.-H., Gregorini L., Parma P., 1995, A&A, 303, 427
Konar C., Saikia D. J., Ishwara-Chandra C. H., Kulkarni V. K., 2004, MNRAS, 355, 845
Konar C., Saikia D. J., Jamrozy M., Machalski J., 2006, MNRAS, 372, 693
Konar C., Jamrozy M., Saikia D. J., Machalski J., 2008, MNRAS, 383, 525
Konar C., Hardcastle M., Croston J., Saikia D. J., 2009, MNRAS, 400, 480
Laing R. A., Peacock J. A., 1980, MNRAS, 190, 903
Leahy J. P., Muxlow T. W. B., Stephens P. W., 1989, MNRAS, 239, 401
Liu R., Pooley G., Riley J. M., 1992, MNRAS, 257, 545
Machalski J., Jamrozy M., Saikia D. J., 2009, MNRAS, 395, 812
Mack K.-H., Klein U., O'Dea C. P., Willis A. G., Saripalli L., 1998, A&A, 329, 431
Murgia M., Fanti C., Fanti R., Gregorini L., Klein U., Mack K.-H., Vigotti M., 1999, A&A, 345, 769
Myers S. T., Spangler S. R., 1985, ApJ, 291, 52
Pacholczyk A. G., 1970, Radio Astrophysics. W. H. Freeman & Co., San Francisco
Parma P., Murgia M., Morganti R., Capetti A., de Ruiter H. R., Fanti R., 1999, A&A, 344, 7
Riley J. M., Pooley G. G., 1975, Mem. R. Astron. Soc., 80, 105
Rudnick L., Katz-Stone D., Anderson M., 1994, ApJS, 90, 955
Saikia D. J., Konar C., Kulkarni V. K., 2006, MNRAS, 366, 1391
Schmidt M., 1965, ApJ, 141, 1
Schoenmakers A. P., Mack K.-H., de Bruyn A. G., Röttgering H. J. A., Klein U., van der Laan H., 2000, A&AS, 146, 293
Schoenmakers A. P., de Bruyn A. G., Röttgering H. J. A., van der Laan H., 2001, A&A, 374, 861
Singal A. K., Konar C., Saikia D. J., 2004, MNRAS, 347, L79
Sirothia S. K., Saikia D. J., Ishwara-Chandra C. H., Kantharia N. G., 2009, MNRAS, 392, 1403
Smith H. E., Spinrad H., 1980, PASP, 92, 553
Spergel D. N. et al., 2003, ApJS, 148, 175
Subrahmanyan R., Saripalli L., 1993, MNRAS, 260, 908
Subrahmanyan R., Saripalli L., Hunstead R. W., 1996, MNRAS, 279, 257
Vigotti M., Grueff G., Perley R., Clark B. G., Bridle A. H., 1989, AJ, 98, 419
Wiita P. J., Gopal-Krishna, 1990, ApJ, 353, 476

This paper has been typeset from a TEX/LATEX file prepared by the author.